Sensors and Materials, Vol. 36, No. 3 (2024) 1081–1091
MYU Tokyo

S & M 3582

Indium Zinc Oxide pH Sensors: Fabrication, Measurement, and Applications

Jung-Lung Chiang[1*] and Yi-Yan Lin[2]

[1]Graduate Institute, Prospective Technology of Electrical Engineering and Computer Science,
National Chin-Yi University of Technology,
No. 57, Sec. 2, Zhongshan Rd., Taiping Dist., Taichung 411030, Taiwan (R.O.C.)
[2]Department of Electronic and Computer Engineering, National Taiwan University of Science and Technology,
No. 43, Keelung Rd., Sec. 4, Da'an Dist., Taipei City 106335, Taiwan (R.O.C.)

(Received October 30, 2023; accepted December 19, 2023)

Keywords: indium zinc oxide, sputtering, EGFET, pH sensor, disposable

In this study, indium zinc oxide (IZO) thin films were deposited at different pressures by RF sputtering. The IZO thin films were examined using X-ray diffraction (XRD), SEM, and AFM instruments. The observed crystal orientations [(100), (101), and (008)] were obtained near 31°. The experimental results also reveal slight height variations on the surfaces of the IZO thin films, with average roughness (Ra) values of 2.431, 3.873, and 5.682 nm for sputtering pressures of 10, 20, and 30 mTorr, respectively. In addition, the IZO/Si sensor head and reference electrode were immersed in buffer solutions with various pH values (1, 3, 5, 7, 9, and 11) to measure pH sensitivity. A series of current–voltage (*I–V*) characteristic curves were obtained using a semiconductor parameter analysis instrument. The pH sensitivity of the IZO extended-gate field-effect transistor (EGFET) was calculated to be approximately 58.9, 56.4, and 52.3 mV/pH for 10, 20, and 30 mTorr sputtering pressures, respectively. The IZO pH-EGFET showed superior pH sensitivity and linear response and has great potential as a disposable pH sensor.

1. Introduction

Over the past decade, the sensing structure of extended-gate field-effect transistors (EGFETs) has been widely studied in related applications such as pH sensing and biomedical sensing.[1–4] The EGFET structure offers several advantages, including low cost, simple packaging, insensitivity to temperature and light, flexibility in sensor head design, and improved long-term stability.[5]

Many studies based on EGFET architecture use oxide-conductive materials as sensing materials, such as indium tin oxide (ITO) or indium zinc oxide (IZO). Both are widely applied as transparent conductive materials owing to their simple and cost-effective deposition process as thin films on various substrates such as silicon wafers, glass, polyethylene terephthalate, and polycarbonate, as well as their desirable optical and electrical characteristics.[6–8] ITO and IZO are commonly used as optically transparent electrodes in displays, solar cells, thin-film

*Corresponding author: e-mail: cjunglung@ncut.edu.tw
https://doi.org/10.18494/SAM4745

ISSN 0914-4935

transistors (TFTs), and other optoelectronic devices owing to their excellent electrical and light transmittance properties.

pH is a critical parameter in studies related to human health, the environment, biomedicine, agriculture, and drinking water. pH sensors with high sensitivity and stability have significant potential in modern life, medicine, industry, and other fields.[5] In recent years, researchers have employed sputtering,[6,9–11] sol-gel,[12,13] pulsed laser deposition,[14] and other methods to prepare IZO thin films for various applications. For instance, a flexible IZO-based neuromorphic transistor with multiple in-plane gate electrodes has been proposed for pH sensing applications.[15] Additionally, Jung *et al.* have successfully demonstrated flexible DNA biosensors using low-temperature solution-processed IZO TFTs, exhibiting superior signal-to-noise ratios and clear quantitative analysis results.[16] Another study aimed to enhance the sensing capabilities of IZO-based TFTs by utilizing an acid-doped chitosan-based biopolymer electrolyte as the gate dielectric, achieving a sensitivity of 57.8 mV/pH through the modulation of the dynamic electric-double-layer charging process.[17] Moreover, Jang *et al.* presented a-IGZO TFT-based EGFETs with a marked sensitivity of 129.1 mV/pH, surpassing the Nernst response.[18] These examples highlight the application of IZO-based TFTs in biosensors, often involving complex sensing element architectures.

In contrast, in this study, we employed a simple EGFET sensing structure comprising an IZO thin film deposited on a silicon substrate (5 × 5 mm^2) using RF sputtering and commercial MOSFET devices. The IZO/Si structure encapsulated with epoxy resin is shown in Fig. 1(d). A 2 × 2 mm^2 sensing window was reserved for pH testing. The IZO/Si sensing structure served as

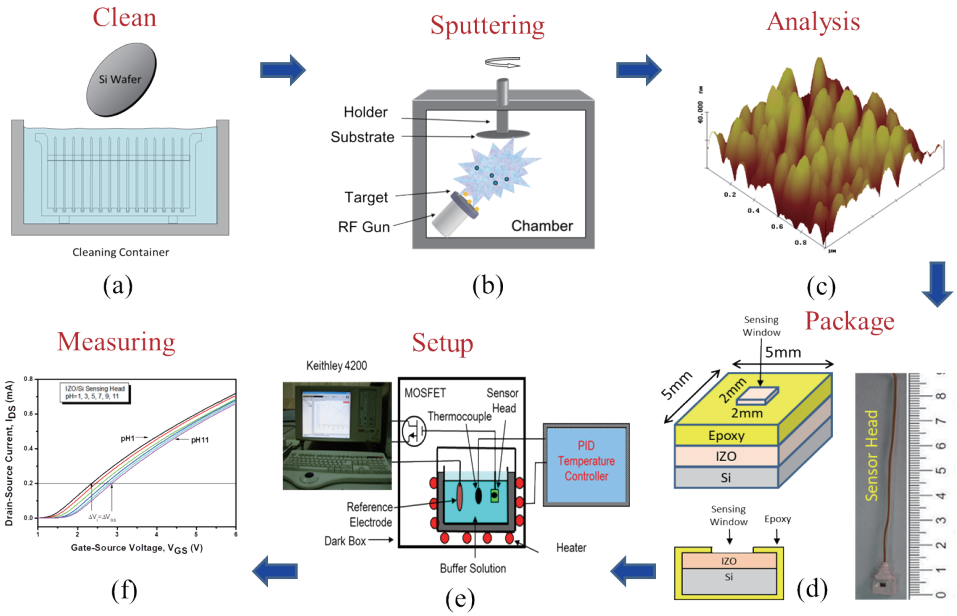

Fig. 1. (Color online) Flowchart of preparation and measurement process.

the pH sensor head connected to the gate of the MOSFET. The current–voltage (*I–V*) characteristics of the IZO pH-EGFET were measured in pH 1–11 buffer solutions, and the results were observed using a semiconductor parameter analyzer. Some results showed a high pH sensitivity and a linear response as shown in Ref. 19. In addition, we also explored the changes in the pH sensing response of the IZO/Si sensing material by adjusting the sputtering pressure. The different surface roughness of the IZO thin film can be achieved by adjusting the sputtering pressure; the effect of the film surface roughness on the pH sensing response was also analyzed. The experimental results showed that the IZO pH-EGFET sensor exhibited a high pH sensitivity ranging from 52 to 59 mV/pH, depending on the sputtering pressure ranging from 10 to 30 mTorr. In addition, the relevant comparisons between this study and Refs. 15 and 18 are shown in Table 1. In this study, the IZO/Si EGFET process is simple and low-cost and can be used for testing a wider range of pH values. The sensor head and MOSFET are separated structures that are more suitable for disposable applications.

2. Experiment, Materials, and Methods

The experimental procedures in this study encompassed several key steps: substrate cleaning, thin-film deposition, material analysis, sensor packaging, measurement setup, and the characterization analysis of the IZO pH-EGFET. A flowchart illustrating the preparation and measurement process is presented in Fig. 1.

2.1 Preparation of IZO thin film

Initially, the silicon substrate underwent a standard cleaning process. A sputtering target composed of In_2O_3-ZnO (90:10 wt%) was utilized. Subsequently, IZO thin films were deposited on the silicon substrate via RF sputtering. The deposition process was conducted using an Ar/O_2 (50/2.5 sccm) gas mixture at total operating pressures of 10, 20, and 30 mTorr, with an RF power of 60 W for a duration of 1 h. The thickness and surface morphology of the IZO thin films were examined using a SEM device (JEOL JSM-6700F). The crystalline orientation of the films was determined using an X-ray diffraction analysis system (SHIMADZU XRD-6000). Additionally, the surface roughness of the films was observed via an AFM device (Digital Instrument Nanoscope III). Furthermore, the surface element composition of the films was analyzed using an Auger electron spectroscopy (AES) system (VG. Microlab 310D). The electrical properties of the IZO films were assessed by the four-point probe technique.

Table 1
Relevant comparisons between this study and Refs. 15 and 18.

Sensing structure	Substrate	Process	Cost	Sensitivity (mV/pH)	Test range	Reference
IZO TFT/n-SiO_2/ITO/PET	PET	complicated	high	37.5	pH 4–10	15
a-IGZO TFT-based EGFET	Si	complicated	high	59.2 (single gate mode) 129.1 (dual gate mode)	pH 3–10	18
IZO/Si EGFET	Si	simple	low	52–59	pH 1–11	This study

2.2. Package of IZO/Si sensor head

Secondly, the completed IZO/Si structure was encapsulated with epoxy resin to form a disposable sensor head. A sensing window area of ~4 mm^2 was specifically reserved for pH-sensing tests.

2.3. IZO pH-EGFET measurement setup

The *I–V* characteristic curve of the IZO pH-EGFET was measured using a semiconductor parameter analysis instrument (Keithley 4200). The pH sensor head was connected to the gate terminal of the MOSFET during the measurement. The IZO pH-EGFET and the Ag/AgCl reference electrode were immersed in buffer solutions with pH values of 1, 3, 5, 7, 9, and 11 for pH detection. To ensure accurate measurements, the entire measurement system was placed inside a black box, and the pH buffer solutions were maintained at room temperature. The measurement setup is depicted in Fig. 1. In addition, the constant voltage and constant current (CVCC) circuit was used to measure the voltage–time (*V–T*) output response curve of the IZO pH-EGFET in the pH 1–11 buffer solutions.

3. Results and Discussion

In this study, the surface morphology and cross section of the IZO thin film deposited at 10 mTorr were examined by SEM. Figure 2 shows the SEM image of the IZO thin film, and Figs. 2(a) and 2(b) present the surface morphology and cross section, respectively. The SEM image revealed a highly dense IZO thin film surface. Additionally, the inset in Fig. 2(b) allows the determination of the film thickness, which was found to be approximately 300 nm. The electrical characteristic of the IZO thin film was measured using a four-point probe to be in the range of 2.5×10^{-4}–3×10^{-5} Ω-cm and observed for deposition at sputtering pressures ranging from 10 to 30 mTorr. In this study, the resistance of the IZO thin film is between 10^{-4} and 10^{-5} Ω-cm, and the film exhibits relatively high voltage stability and conduction efficiency under low resistance conditions. Generally, an IZO thin film has a high conductivity and is very important for measuring the pH response of the EGFET structure.

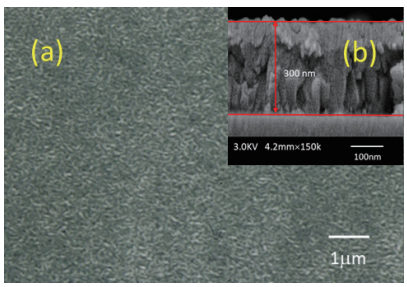

Fig. 2. (Color online) SEM image of IZO thin film: (a) top view of surface morphology and (b) cross section.

The crystalline orientation of the IZO thin film was determined through XRD analyses, as shown in Fig. 3. The experimental results exhibited a peak near 31°, indicating the presence of polycrystalline $Zn_2In_2O_5$. The observed crystal orientations were found to be consistent with those reported in Refs. 20 and 21, specifically (100), (101), and (008).

The surface elemental composition and depth distribution of the IZO/Si sample were analyzed via AES, as illustrated in Fig. 4. Figures 4(a) and 4(b) present the original and differential signals of the AES analysis for the preparation of IZO thin films at a sputtering pressure of 10 mTorr, respectively. Notably, the differential signals clearly distinguish the amplitudes of the three elements: indium (In), oxygen (O), and zinc (Zn). The peak signals indicate the composition of the film as indium zinc oxide, confirming the presence of indium, zinc, and oxygen in the film.

Furthermore, we employed an Ar sputtering gun to thin down the material and analyze the Auger spectra in depth. The objective was to carry out a concentration-depth analysis of each

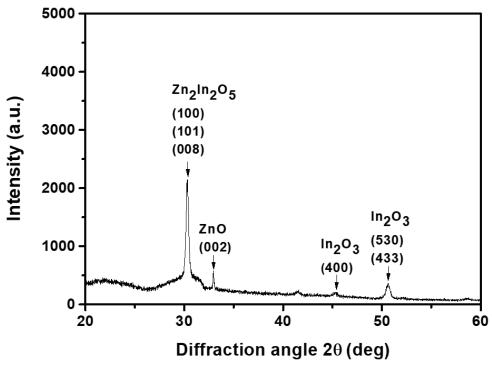

Fig. 3. X-ray diffraction profile of IZO thin film.

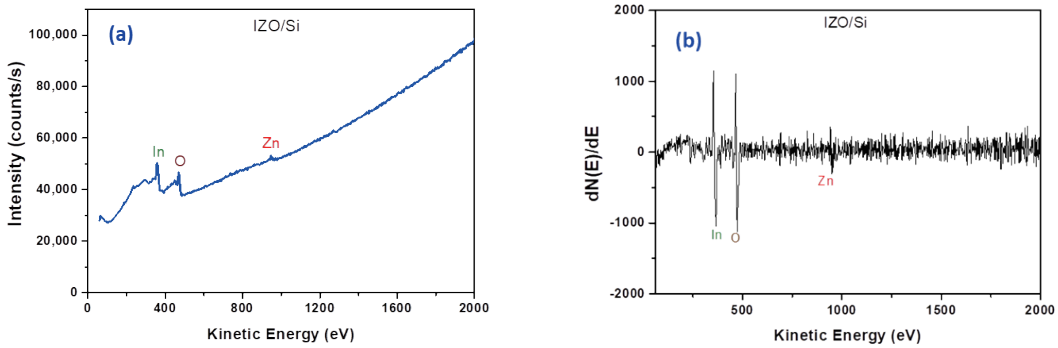

(a) (b)

Fig. 4. (Color online) AES results of IZO/Si sample: (a) original and (b) differential signals.

element at various material depths. Figure 5 presents a plot depicting the relationship between Auger intensity and sputtering time. The vertical axis denotes counts/eV/s, whereas the horizontal axis represents time (s), corresponding to the duration of ion beam bombardment on the thin film. The experimental results clearly demonstrate that the element concentration in the thin film follows the trend of In > Zn, consistent with the composition of the sputtering target, In_2O_3-ZnO (90:10 wt%). Furthermore, as the ion beam bombardment time increases, the thin film structure becomes apparent as IZO/Si. Figure 5 also indicates that the proportions of In, O, and Zn elements in the film remain relatively constant with increasing ion beam bombardment time, showcasing the excellent compositional uniformity of the prepared IZO thin film.

As shown in Fig. 6, we observed the surface roughness of the IZO thin film deposited on a Si substrate at different sputtering pressures (10, 20, and 30 mTorr) by AFM. The experimental results reveal slight height variations on the surface of the IZO thin film, with average roughness (Ra) values of 2.431, 3.873, and 5.682 nm for sputtering pressures of 10, 20, and 30 mTorr, respectively. This indicates the effects of different sputtering pressures on the surface roughness of the IZO thin film. Figure 7(a) illustrates the relationship between the sputtering pressure and average surface roughness of the IZO thin film, showing that the surface particles of the IZO thin film become larger and its average roughness increases with the sputtering pressure. These findings align with the results reported in Refs. 22 and 23, confirming that the surface becomes smoother as the sputtering pressure decreases.

Next, we discuss the response trend of the *I–V* characteristic curve of the IZO pH-EGFET prepared at sputtering pressures of 10, 20, and 30 mTorr. Figure 8 shows a series of *I–V* curves of the IZO pH-EGFET obtained using a semiconductor parameter analysis instrument (Keithley 4200) in buffer solutions ranging from pH 1 to 11. With the drain–source current of the IZO pH-EGFET set at 0.2 mA, the sensor recorded varying threshold voltage (ΔV_t) or gate–source voltage (ΔV_{GS}) values. These values exhibited a linear shift to the right with an increase in pH. In other words, when the sensor head was immersed in a solution with a high pH, the pH-EGFET showed a high threshold voltage. The I_{DS}–V_{GS} characteristic curve shifts to the right as the pH of the buffer solution increases, indicating the pH sensitivity of the sensor. The pH sensitivity can be expressed as

$$\text{pH sensitivity} = V_x - V_y / pH_x - pH_y = \Delta V_t / \Delta pH = \Delta V_{GS} / \Delta pH, \tag{1}$$

where V_x and V_y can also represent the different threshold voltages when the pH sensor is placed in pH_x and pH_y buffer solutions.

According to the aforementioned information, the varying threshold voltage was recorded, allowing for the calculation of pH sensitivity from Fig. 8. Thus, different gate–source voltages (V_{GS}) of the sensor in various pH buffer solutions were obtained. The pH sensitivity response and linear regression curves are plotted in Fig. 9. In this study, different sputtering pressures were adjusted to deposit the IZO thin films. The experimental results indicate sensitivities of approximately 58.9, 56.4, and 52.3 mV/pH for sputtering pressures of 10, 20, and 30 mTorr, with linearities of 0.9997, 0.9989, and 0.9953, respectively. These experimental findings are depicted in Figs. 7(b) and 7(c). It can be observed that the pH sensitivity decreases as the sputtering

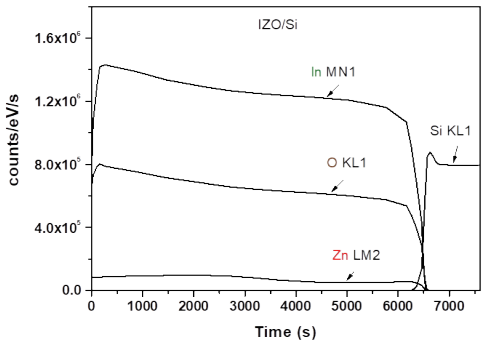

Fig. 5. (Color online) Depth analysis plot of AES for IZO/Si sample.

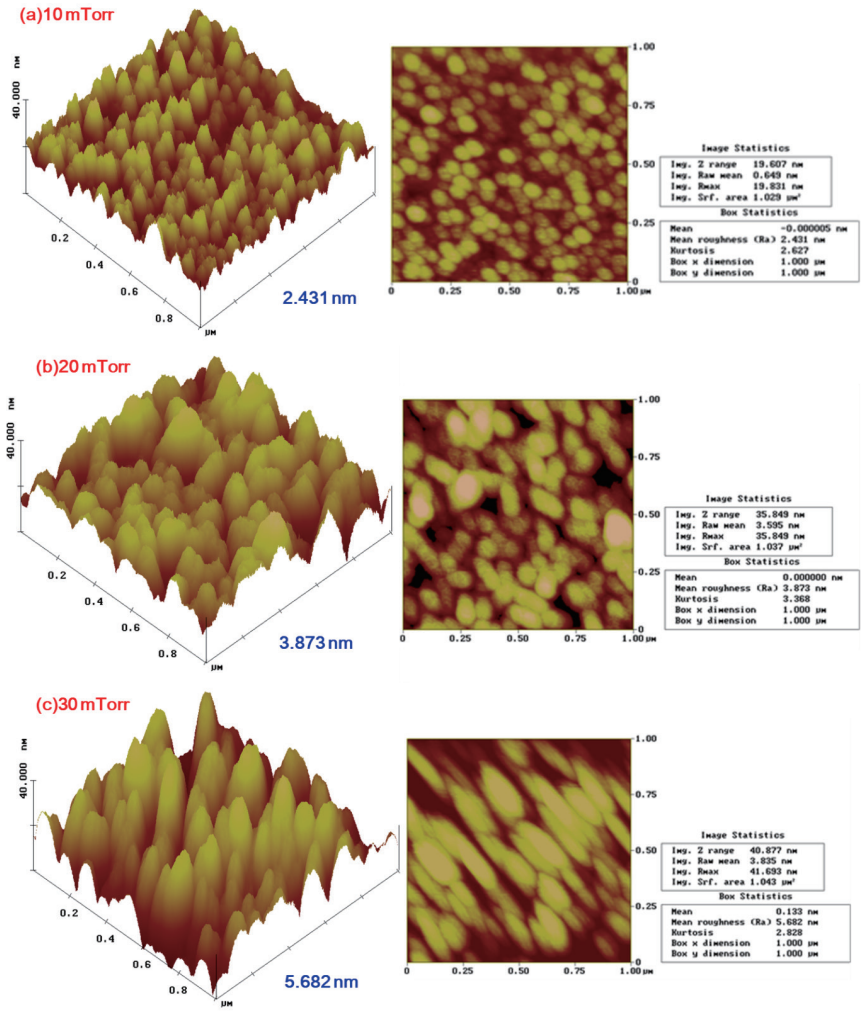

Fig. 6. (Color online) Surface roughness of IZO thin film measured and compared at different sputtering pressures: (a) 10, (b) 20, and (c) 30 mTorr.

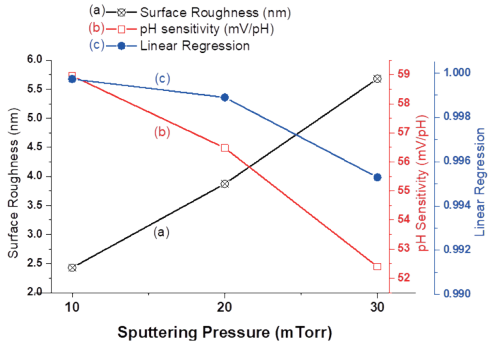

Fig. 7. (Color online) IZO thin films deposited at 10, 20, and 30 mTorr sputtering pressures: (a) surface roughness, (b) pH sensitivity, and (c) linear regression.

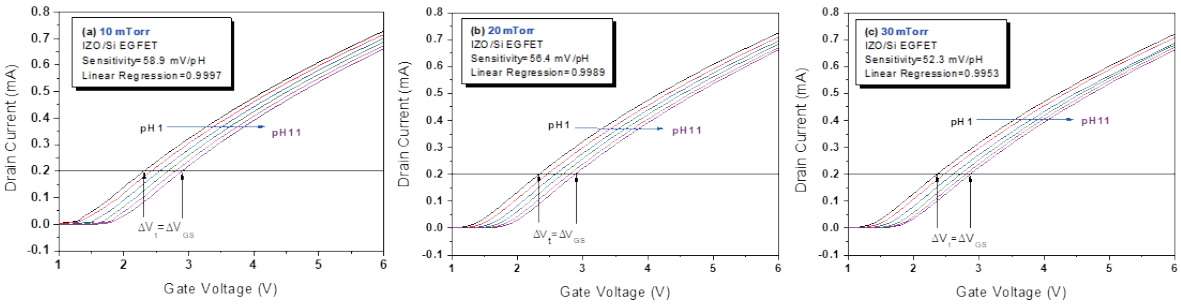

Fig. 8. (Color online) *I–V* curve of IZO pH-EGFET investigated in pH 1–11 buffer solutions: (a) 10, (b) 20, and (c) 30 mTorr.

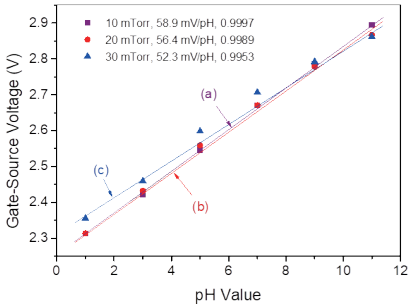

Fig. 9. (Color online) pH response of IZO pH-EGFET deposited at sputtering pressures of (a) 10, (b) 20, and (c) 30 mTorr and evaluated on the basis of pH sensitivity and linear regression.

pressure increases, and the linearity also decreases accordingly. Additionally, an increase in sputtering pressure leads to a larger surface roughness of the IZO film, resulting in a decrease in pH sensitivity. These results align with the experimental findings reported in Refs. 21 and 22. The experimental results also show that the sensing ability of the film and the amount of adsorption and hydrogen bonding on the surface are the main factors affecting the sensitivity. By varying the surface roughness, the sensing ability will be affected. The flatter the surface, the higher the sensing performance. In addition, a flatter sensing film surface makes it easier to generate hydrogen ion adsorption bonds, thereby improving the sensing capability.

In addition, the IZO pH sensor is placed in buffer solutions of pHs 1, 3, 5, 7, 9, and 11, and a CVCC circuit [Fig. 10(a)] is used to measure the voltage–time (*V*–*T*) output response curve. Here, the drain voltage was set to 0.2 V and the drain current to 0.2 mA for pH testing at 25 ± 0.1°C. The experimental results are shown in Fig. 10(b). It can be seen that as pH increases, the output voltage shifts upward. After 120 s, the output voltage response value is recorded and calculated. The pH sensitivity of the IZO pH-EGFET is approximately 52 mV/pH.

In this study, temperature is also an important influencing factor. The temperature versus time of each pH buffer was monitored, as shown in Fig. 10(c). The measurement results indicate that the temperature of the pH buffer solutions was maintained at 25.1 °C, with no significant change observed. Therefore, the temperature effect can be temporarily ignored.

Reference 19 mentions that the pH-sensing characteristics of the IZO, AZO, ITO, RuO_2, and ZnO sensing materials were compared on the basis of EGFET. According to the comparison results,[19] the IZO thin film deposited on a Si substrate by RF sputtering demonstrates excellent pH sensitivity, ranging from 52 to 59 mV/pH in the pH range of 1 to 11 in our study. These marked sensing properties of IZO can be applied to pH detection and biosensing applications. Finally, we re-summarized the previous description and experimental results. The IZO thin film was deposited on a silicon substrate by RF sputtering; the sputtering pressure was set to 10–30 mTorr, the sputtering power to 60W, the substrate temperature to 30 °C, and the sputter chamber of the reaction gas of Ar/O_2 to 50/2.5 sccm for 1 h sputtering. The IZO pH sensor has a high pH sensitivity and good linearity.

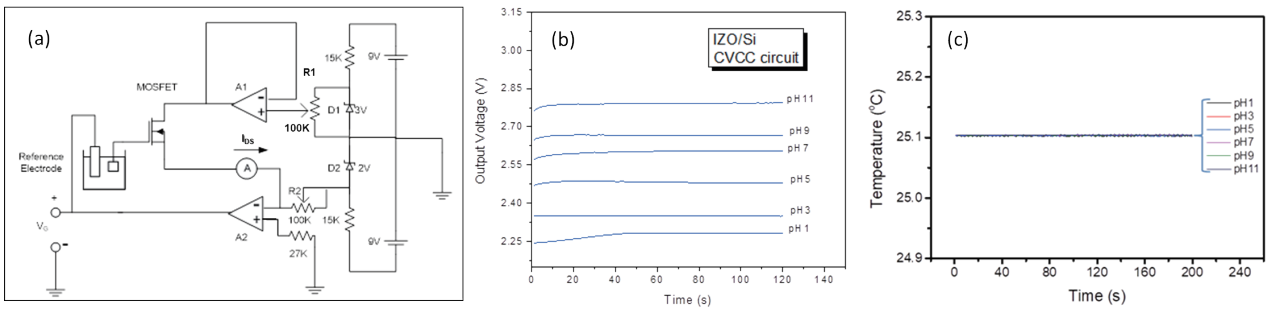

Fig. 10. (Color online) IZO pH-EGFET was measured in pHs 1, 3, 5, 7, 9, and 11 buffer solutions: (a) CVCC circuit, (b) output voltage curve, and (c) temperature and time curve.

4. Conclusions

In this study, IZO crystallographic properties and composition have been demonstrated using XRD and AES instruments. The IZO pH-EGFET showed high pH sensitivity and an excellent linear response. High-performance IZO-based pH sensors are fabricated by RF sputtering at depositing pressures ranging from 10 to 30 mTorr. We used an I-V semiconductor measurement system and a CVCC circuit to verify the pH sensing response. The IZO pH-EGFET demonstrated excellent pH sensitivity, ranging from 52 to 59 mV/pH, and exhibited a linear pH response with a close-to-unity linear regression coefficient in the pH range of 1−11. In addition, the electrical characteristic of the IZO thin film was measured to be in the field of 10^{-4}–10^{-5} Ω-cm. The surface roughness of the IZO thin film plays a significant role in the pH-sensing characteristics, with minor surface roughness; that is, the flatter the surface, the higher the sensing performance, leading to higher sensitivity. Compared with other sensing materials, the IZO pH-EGFET showed a superior pH response. Consequently, the IZO pH-EGFET has excellent potential as a disposable pH sensor or biosensor and can find applications in environmental monitoring, industrial processes, and water pollution monitoring in the future.

Acknowledgments

The authors thank the National Chin-Yi University of Technology for their financial (No. NCUT23-T-CP-012) and instrument equipment support.

References

1 J. L. Wang, P. Y. Yang, T. Y. Hsieh, C. C. Hwang, and M. H. Juang: J. Nanomater. **2013** (2013) 152079. https://doi.org/10.1155/2013/152079
2 J. L. Chiang, S. S. Jhan, S. C. Hsieh, and A. L. Huang: Thin Solid Films **517** (2009) 4805. https://doi.org/10.1016/j.tsf.2009.03.050
3 N. Mokhtarifar, F. Goldschmidtboeing, and P. Woias: IET Micro Nano Lett. **13** (2018) 1525. https://doi.org/10.1049/mnl.2018.5240
4 N. M. Ahmed, F. A. Sabah, N. H. Al-Hardan, M. A. Almessiere, S. M. Mohammad, W. F. Lim, M. Jumaah, A. K. M. Shafiqul Islam, Z. Hassan, H. J. Quah, and N. Afzal: Semicond. Sci. Technol. **36** (2021) 045027. https://iopscience.iop.org/article/10.1088/1361-6641/abe914
5 L. Manjakkal, D. Szwagierczak, and R. Dahiya: Prog. Mater. Sci. **109** (2020) 100635. https://doi.org/10.1016/j.pmatsci.2019.100635
6 D. Lee, A. Lee, and H. D. Kim: IEEE Access **10** (2022) 77170. https://ieeexplore.ieee.org/document/9833488
7 J. L. Chiang, S. W. Li, B. K. Yadlapalli, and D. S. Wuu: Vacuum **186** (2021) 1. https://doi.org/10.1016/j.vacuum.2021.110046
8 A. K. Akhmedov, E. K. Murliev, A. S. Asvarov, A. E. Muslimov, and V. M. Kanevsky: Coatings **12** (2022) 1. https://www.mdpi.com/2079-6412/12/10/1583
9 J. Park, Y. Lim, M. Jang, S. Choi, N. Hwang, and M. Yi: Mater. Res. Bull. **96** (2017) 155. https://doi.org/10.1016/j.materresbull.2017.05.001
10 H. E. Silva-Lopez, B. S. Marcelino, A. Guillen-Cervantes, O. Zelaya-Angel, and R. Ramirez-Bon: Mater. Res. **21** (2018) 1. https://doi.org/10.1590/1980-5373-MR-2018-0224
11 L. Gomes, A. Marques, A. Branco, J. Araújo, M. Simões, S. Cardoso, F. Silva, I. Henriques, C. A. T. Laia, and C. Costa: Displays **34** (2013) 326. https://doi.org/10.1016/j.displa.2013.06.004
12 J. F. Tang, L. C. Chen, Z. L. Tseng, and S. Y. Chu: J. Nanoelectron. Optoelectron. **12** (2017) 849. https://doi.org/10.1166/jno.2017.2077

13 I. Choudhary, and Deepak: J. Sol-Gel Sci. Technol. **100** (2021) 132. https://doi.org/10.1007/s10971-021-05615-w
14 M. Socol, N. Preda, A. Stanculescu, C. Breazu, C. Florica, O. Rasoga, F. Stanculescu, and G. Socol: Appl. Phys. A **123** (2017) 371. https://doi.org/10.1007/s00339-017-0992-4
15 N. Liu, L. Q. Zhu, P. Feng, C. J. Wan, Y. H. Liu, Y. Shi, and Q. Wan: Sci. Rep. **5** (2015) 18082. https://doi.org/10.1038/srep18082
16 J. Jung, S. J. Kim, K. W. Lee, D. H. Yoon, Y. G. Kim, H. Y. Kwak, S. R. Dugasani, S. H. Park, and H. J. Kim: Biosens. Bioelectron. **55** (2014) 99. https://doi.org/10.1016/j.bios.2013.11.076
17 N. Liu, L. Gan, Y. Liu, W. Gui, W. Li, and X. Zhang: Appl. Surf. Sci. **419** (2017) 206. https://doi.org/10.1016/j.apsusc.2017.04.248
18 H. J. Jang, J. G. Gu, and W. J. Cho: Sens. Actuators, B **181** (2013) 880. https://doi.org/10.1016/j.snb.2013.02.056
19 J. L. Chiang and Y. Y. Lin: Proc. 2023 6th Int. Symp. Computer, Consumer and Control (IS3C), 2023 IEEE Xplore. https://doi.org/10.1109/IS3C57901.2023.00070
20 T. Minami, H. Sonohara, T. Kakumu, and S. Takata: Japn. J. Appl. Phys. **34** (1995) L971. https://iopscience.iop.org/article/10.1143/JJAP.34.L971
21 T. Minami, T. Kakumu, Y. Takeda, and S. Takata: Thin Solid Films **317** (1998) 326. https://doi.org/10.1016/S0040-6090(97)00548-8
22 J. C. Chou and C. N. Hsiao: Sens. Actuators, B **65** (2000) 237. https://doi.org/10.1016/S0925-4005(99)00446-3
23 W. Lim, Y. L. Wang, F. Ren, D. P. Norton, I. I. Kravchenko, J. M. Zavada, and S. J. Pearton: Appl. Surf. Sci. **254** (2008) 2878. https://doi.org/10.1016/j.apsusc.2007.10.032

About the Authors

Jung-Lung Chiang received his Ph.D. degree from National Sun Yat-sen University, Taiwan, in 2002. Since 2022, he has been an associate professor at the National Chin-Yi University of Technology, Taichung, Taiwan. His research interests include nanomaterials, thin film technology, sensor applications, photodetector, and micro-LED. (cjunglung@ncut.edu.tw)

Yi-Yan Lin received his Ph.D. degree from National Taiwan University of Science and Technology, Taiwan, in 2011. Since 2012, he has been an senior engineer at AU Optronics (AUO). His research interests include thin film, sensor applications, and micro-LED.